**ORIGINAL PAPER**

# Evaluating Stability and Activity of SARS-CoV-2 PLpro for High-throughput Screening of Inhibitors

**Rimanshee Arya**[1,2] · **Vishal Prashar**[1] · **Mukesh Kumar**[1,2]

## Abstract

Because of the essential roles of SARS-CoV-2 papain-like protease (PLpro) in the viral polyprotein processing and suppression of host immune responses, it is a crucial target for drug discovery against COVID-19. To develop robust biochemical methodologies for inhibitor screening against PLpro, extensive characterization of recombinant protein is important. Here we report cloning, expression, and purification of the recombinant SARS-CoV-2 PLpro, and explore various parameters affecting its stability and the catalytic activity. We also report the optimum conditions which should be used for high-throughput inhibitor screening using a fluorogenic tetrapeptide substrate.

**Keywords** SARS-CoV-2 · COVID-19 · Papain-like protease · Enzyme activity · Aggregation · Stability

## Introduction

Since the first report of novel coronavirus disease (COVID-19) from Wuhan, China in December 2019, it has spread rapidly to most of the countries around the world [1]. The large-scale spread of COVID-19 across the continents has put a significant burden on the health care systems and the world economy. The disease is caused by a coronavirus, named severe acute respiratory syndrome coronavirus 2 (SARS-CoV-2). Around two-thirds of the viral genome encode for two large overlapping polyproteins, pp1a and pp1ab, which are subsequently cleaved to individual non-structural proteins (NSPs) by two virus-encoded proteases, namely papain-like protease (PLpro) and chymotrypsin-like protease (CLpro or main protease, Mpro or NSP5) [2, 3]. While Mpro cleaves the polypeptide sequence from NSP4 to NSP16 at 11 places, PLpro cleaves the sequence from NSP1 to NSP4 at three places. The cleavage of the viral

polyproteins to different NSPs is essential for the formation of the replication-transcription complex in the host cell for viral replication. Therefore, specific inhibitors of these viral proteases could be developed as potential therapeutics against COVID-19 [4]. PLpro, apart from cleaving the viral polyproteins, is also involved in the suppression of the host immune responses through deubiquitination and deISG15lyation activities in the infected cells [5]. Therefore, PLpro as a therapeutic target has the dual advantage of suppressing viral replication in the host cell and preventing the dysregulation of host immune responses caused by its deubiquitination and deISG15lyation activities.

PLpro is one of the structural domains of a large (~200 kDa) multidomain non-structural protein 3 (NSP3). It is a cysteine protease having a recognition sequence, LXGG↓X, where X is any amino acid. SARS-CoV-2 PLpro shares 82.59% and 30.06% sequence identity with PLpro of SARS-CoV and MERS-CoV, respectively. In the past year several structural, functional, and inhibition studies of PLpro from SARS-CoV-2 have been carried out [6–11]. It has a right-hand architecture containing the thumb, palm, and fingers subdomains similar to PLpro from SARS-CoV and MERS-CoV. The active site, located at the interface of fingers and palm subdomains, contains a catalytic triad of C111, H273, and D293 residues. A flexible loop (BL2) is present near the entrance of the active site cavity which plays an important role in inhibitor/substrate binding.

✉ Vishal Prashar
  vishalp@barc.gov.in

✉ Mukesh Kumar
  mukeshk@barc.gov.in

1 Protein Crystallography Section, Radiation Biology & Health Sciences Division, Bhabha Atomic Research Centre, Mumbai 400085, India

2 Homi Bhabha National Institute, Anushakti Nagar, Mumbai 400094, India

Although PLpro shows significantly enhanced activity against ubiquitin and ISG15 based substrates, small peptide substrates are very useful for high-throughput screening of potential inhibitors. The optimum conditions for the enzyme assays with a small peptide substrate, however, have not yet been reported. Here, we explore various parameters affecting enzymatic assays using a fluorogenic tetrapeptide substrate, Z-LRGG-AMC, mimicking the cleavage site sequence for the deubiquitination and deISG15ylation. Upon cleavage, the AMC moiety (7-amino-4-methyl-coumarin) gives high fluorescence which can be monitored continuously. Apart from catalytic efficiency, the thermal stability and the aggregation behavior of the enzyme have also been investigated under various conditions.

## Materials and Methods

### Cloning, Expression, and Purification of PLpro

The nucleotide sequence for SARS-CoV-2 PLpro corresponding to the amino acids sequence 746-1064 of NSP3 (NCBI reference sequence: YP_009725299) was codon-optimized for expression in *Escherichia coli* (Supplementary data 1 & 2). The sequence was synthesized and cloned into the pET28a vector (Novagen) using *Nde*1 and *Bam*H1 restriction sites. The sequence upstream of the cloned gene encodes an N-terminal hexahistidine-tag and a thrombin cleavage site (Supplementary data 3). *E. coli* BL21 (DE3) cells were transformed with the recombinant plasmid and the culture was grown in Luria- Bertani medium at 37 °C until the $OD_{600}$ reached 0.8–1.0. The protein expression was induced by adding IPTG (Isopropyl β-D-1 thiogalactopyranoside) to a final concentration of 0.5 mM along with 100 μM $ZnSO_4$ and the culture was grown overnight at 19 °C. The cells were harvested by centrifugation at $6000 \times g$, resuspended in lysis buffer (20 mM Tris pH 8.5 containing 300 mM NaCl, 10 mM imidazole, 10 mM DTT, 1.0 μM $ZnSO_4$, and 1 mg/ml lysozyme), and lysed by sonication. The lysate was centrifuged at $10,000 \times g$ for 30 min at 4 °C. The supernatant was loaded onto a pre-equilibrated Ni-NTA column (Roche) and binding was carried out on a rocker at 4 °C for 90 min. The beads were washed twice with wash buffer (20 mM Tris, 300 mM NaCl, 20 mM Imidazole, 10 mM DTT, pH 8.5) and the protein was eluted with elution buffer (20 mM Tris, 300 mM NaCl, 250 mM imidazole, 10 mM DTT, pH 8.5). The eluted protein was dialyzed overnight against dialysis buffer (50 mM HEPES, 100 mM NaCl, 10 mM DTT, pH 7.5) at 4 °C. The purity of the protein was checked on 12% SDS-PAGE.

### Size-Exclusion Chromatography

Size-exclusion chromatography was carried out on a Superdex 200 increase 10/300 gel filtration column (GE Healthcare) using column elution buffer (50 mM HEPES, 100 mM NaCl, 5 mM DTT, pH 7.5). The column was calibrated using standard proteins (Ribonuclease 13 kDa, Carbonic anhydrase 29 kDa, Ovalbumin 43 kDa, and Conalbumin 75 kDa) to estimate the oligomerization state of eluted PLpro.

### Dynamic Light Scattering

Dynamic light scattering (DLS) experiments were carried out on Zetasizer Nano-ZS instrument (Malvern Pananalytical Ltd., UK). The purified protein was used at a concentration of one mg/ml in different buffers with and without the reducing agents. The measurements were carried out in low volume disposable sizing cuvette (ZEN0112 of Malvern, UK) at 20 °C. The samples were equilibrated at 20 °C for 30 s followed by three measurements, with every measurement having 15 runs of 10 s each. The scattered light was measured at a backscattering angle of 173°.

### Differential Scanning Fluorimetry

Differential scanning fluorimetry (DSF) measurements were performed in a skirted 96-well plate (Bio-Rad laboratories, Inc.) using CFX Touch real-time PCR detection system (Bio-Rad laboratories, Inc.). The reaction mixture contained 2.7 μM protein in different buffers and SYPRO orange dye (Sigma Life Science) at a final concentration of 5X. The excitation and emission wavelengths were set using FRET channel at 455–485 nm and 567–596 nm, respectively. To initiate measurements, the reaction mixture was equilibrated at 20 °C for 3 min. The mix was then heated to 95 °C at a ramping rate of 2 °C/min. The melting temperature ($T_m$) was calculated from the maxima of the first derivative plot of the fluorescence data.

### Enzymatic Assays

Enzymatic assays of PLpro were carried out using fluorogenic tetrapeptide substrate, Z-Leu-Arg-Gly-Gly-AMC (Biotechne, Cat. No. S-100-05 M), on POLARstar Omega microplate reader (BMG Labtech, Germany). Experiments were performed in 96-well black non-treated plates (Thermo Scientific, Denmark) using excitation and emission filters of 355 nm and 430 nm, respectively. The assays were performed in a reaction volume of 100 μl containing 0.1 mg/ml bovine serum albumin (BSA). The enzyme was used at an optimized concentration of 100 nM with varying amounts of the substrate. The fluorescence data were collected and the

initial rate of change of fluorescence was calculated from the linear portion of the fluorescence versus time plots (typically during the initial 20–30 min). The initial rate of product formation (i.e., initial velocity) was calculated using a calibration curve for AMC. To prepare the calibration curve, different concentrations (2–100 μM) of the substrate were incubated with 10 μM enzyme and measurements were taken when there was no further increase in fluorescence. The kinetic parameters of the enzymatic activity were calculated using the Lineweaver–Burk plot.

## Results & Discussion

### Purification, Oligomeric State, and Aggregation Behavior of PLpro

The recombinant SARS-CoV-2 PLpro was successfully expressed in *E. coli* BL21 (DE3) cells. The protein was purified to high purity and homogeneity as confirmed by SDS-PAGE and size-exclusion chromatography (Fig. 1a and b). Around 20 mg protein could be obtained after chromatography from one liter of bacterial culture.

The oligomeric state of the purified protein was investigated using size-exclusion chromatography and dynamic light scattering. The size-exclusion chromatogram showed the protein elutes at 16 ml from Superdex 200 increase column corresponding to the monomeric form (Fig. 1b and Supplementary Fig. S1). The DLS experiments showed that the protein preparation was homogeneous with hydrodynamic diameter of 7.7 nm in 20 mM Tris, pH 8.5, and 10 mM BME. In the absence of any reducing agent, the protein was found to form large aggregates. The aggregated

state, however, could be reverted to the normal state by adding a reducing agent, 10 mM BME/5 mM DTT (Fig. 1c). At lower pHs (8.0, 7.5, 7.0, and 6.5), though aggregation was not observed immediately in absence of a reducing agent, there was a gradual increase in the aggregated fraction when experiments were performed over a few hours at 20 °C.

The reversibility of aggregation by adding a reducing agent suggests the potential role of some cysteine residue(s). Out of 11 cysteines in PLpro, one cysteine (C111) is a part of the catalytic triad and four cysteines (C189, C192, C224, C226) are present in the finger region, coordinating to a $Zn^{2+}$ ion. Zinc has been reported to be crucial for structural stability and activity of the protein [12, 13]. Since our later experiments showed that the addition of EDTA (up to 2 mM) did not abolish the enzymatic activity of PLpro, zinc ion is assumed to be tightly bound to the cysteines of the finger region. Therefore, those cysteines are unlikely to be involved in making intermolecular interactions. Among the remaining six cysteines (C148, C155, C181, C260, C270, C284), only C270 is exposed to the surface in most of the reported crystal structures with its side chain pointing outwards, making it a potential residue responsible for the intermolecular interactions. Interestingly, C270 was found to be making intermolecular interaction in a few structures of SARS-CoV-2 PLpro. In one of the structures (PDB id: 7JN2), C270 (presumably as a thiolate ion) makes ionic interaction with a positively charged K92 from another protein molecule while in another structure (PDB id: 6W9C), the intermolecular interactions involving C270 is mediated through a metal ion (Zn). It is likely that the aggregate formed through intermolecular interactions in solution is also mediated by C270, which gets reversed by reducing agent (BME/DTT). The suggested pKa of C270 has been reported to be 6.7, [14]
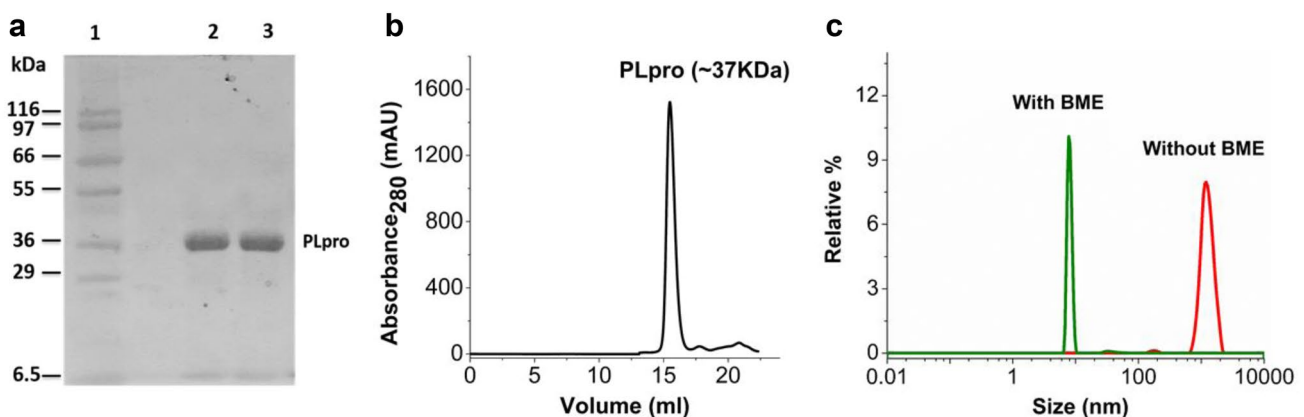


**Fig. 1** Purification and characterization of SARS-CoV-2 PLpro. **a** 12% SDS-PAGE *Lane 1*: Broad-range protein markers (New England Biolabs), *Lane 2:* Purified protein (5 μg) after Ni-NTA chromatography, *Lane 3:* Purified protein (5 μg) after gel filtration chromatography. The gel was stained with coomassie blue. **b** Size-exclusion chro- matography to determine the oligomeric state. **c** DLS experiments showing particle size distribution at pH 8.5, Green: with 10 mM BME, Red: without BME. The aggregated state (red) reverts to the normal state (green) on addition of 10 mM BME

making it more prone to oxidation at higher pH (8.5). This is consistent with our observation that the aggregate formation is faster at pH 8.5 than 6.5. Though C270 from two protein molecules can form a disulfide bond, such interaction would lead to the formation of a protein dimer. The observation that the protein forms larger aggregate in the absence of reducing agent suggests that either a few more cysteines are involved in the formation of a network of intermolecular disulfide bonds, or the thiolate ion of C270 makes ionic interaction with a positively charged residue (like Lys) of another protein molecule.

## Stability of PLpro—DSF Experiments

Thermal stability of PLpro was explored in different buffers with varying amounts of salt (NaCl) by recording the DSF data (Fig. 2). It was found that between pH 4.0–5.0, the fluorescence values were very high at the starting temperature (20 °C) and then decreased gradually on heating, probably due to protein aggregation. It suggests that at these acidic pHs, the protein is partially unfolded and the dye binds to the exposed hydrophobic patches of the protein giving a high fluorescence. However, as the pH increases above 5.5, the hydrophobic patches tend to get buried and a distinct phase transition is observed as the temperature increases from

20 °C to 95 °C. The starting fluorescence is close to 6000 at pH 6.0 which gradually decreases to about 5000 at pH 7.5 and then increases again to about 6000 at pH 8.5 and above. These experiments show the protein is most stable in the pH range 6.5–8.0. Though there was no significant effect of salt (NaCl) on the $T_m$, it was found that the protein precipitates in absence of any salt during long-term storage. The best pH for long-term storage was found to be 7.5 with an addition of 100 mM NaCl to prevent aggregation. Increasing the salt concentrations beyond 100 mM had no significant benefit in preventing the aggregation. The effect of reducing agent (DTT) on protein stability was explored at pH 7.5 with 100 mM NaCl. Though the reducing agent was found to decrease the starting fluorescence slightly, there was no significant effect on the $T_m$ (Fig. 2, last panel). However, for long-term storage, 5 mM DTT was found to be useful to prevent protein aggregation.

## Enzymatic Activity of PLpro

The enzymatic assays of PLpro using a fluorogenic tetrapeptide substrate (Z-LRGG-AMC) were carried out under various conditions. The enzyme concentration for the assays was optimized where the conversion of 10% of the substrate to the product can be recorded in a reasonable time. The
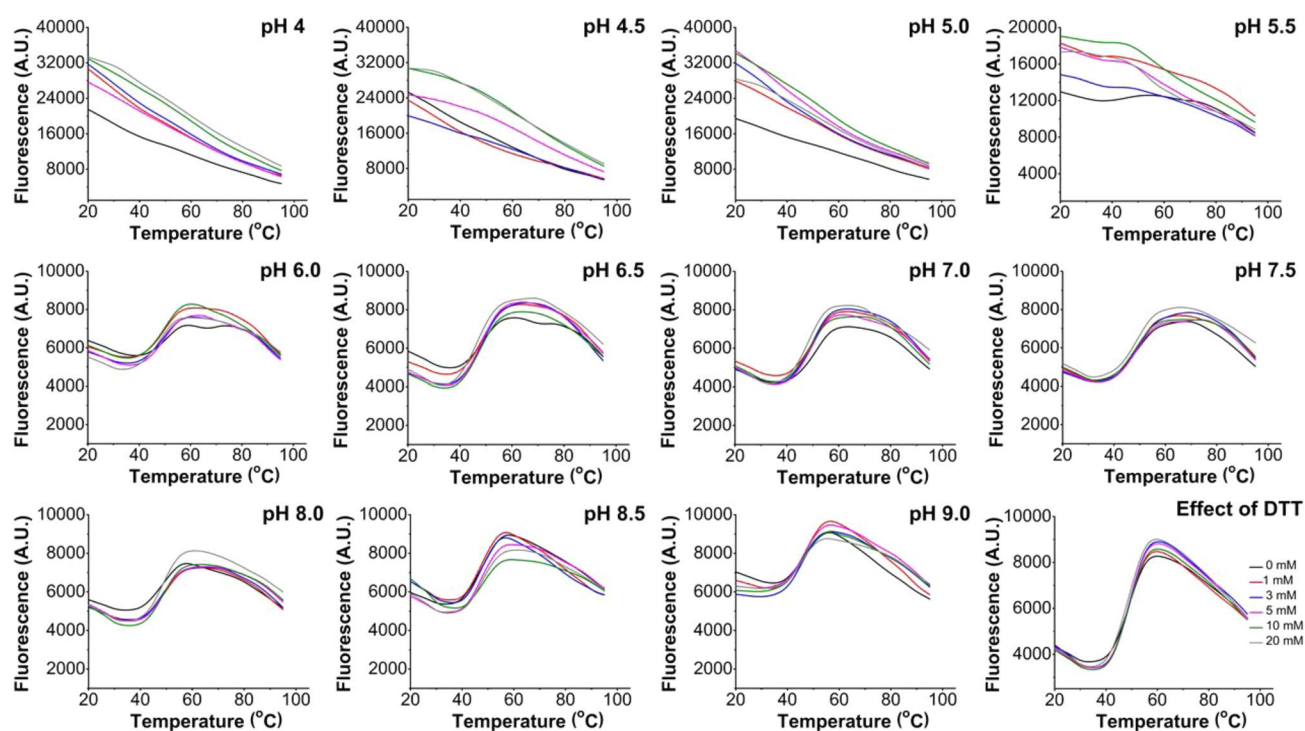


**Fig. 2** Thermal stability assay at different pHs, salt (NaCl) and reducing agent (DTT) concentrations using DSF. At lower pHs (4.0–5.0), the protein is partially unfolded leading to high fluorescence signal of SYPRO orange at the starting temperature (20 °C). At each pH, the curve for different NaCl concentrations are shown in different colors.

Black colored line: 0 mM NaCl, red colored line: 50 mM NaCl, blue colored line: 100 mM NaCl, magenta colored line: 150 mM NaCl, green colored line: 200 mM NaCl, and gray colored line: 500 mM NaCl

optimum enzyme concentration was found to be 100 nM and this concentration was used in all the subsequent assays.

## Dependence of Enzymatic Activity on pH and Temperature

Since pH influences the protonation states of the enzyme and the substrate, it is one of the most important parameters affecting the enzymatic activity. The effect of pH on the enzymatic activity of PLpro was investigated using two approaches. In the first approach, experiments were performed in 50 mM sodium phosphate buffer in the pH range, 4.0–9.5 (Fig. 3a). The enzymatic reactions were performed with varying amounts of the substrate (2–100 μM) in presence of 100 mM NaCl. It was found that in the acidic pH range (4.0–5.0), the enzyme was almost inactive. The observation is consistent with the DSF data suggesting the protein is not folded properly at these pHs. The best efficiency of the enzyme ($k_{cat}/K_m$) was found to be at pH 6.5.

In the second approach, the experiments were performed in 50 mM concentration of different buffers, namely sodium acetate (pH 4.0–5.0), MES (pH 5.5–6.5), HEPES (pH 7.0, 7.5), and Tris (pH 8.0–9.0) in presence of 100 mM NaCl. The enzyme was found to be almost inactive in the acidic pH range (4.0–5.0), consistent with the results from phosphate buffer. Above pH 5.5, the enzyme was found to be active over a wide range of pHs (Fig. 3b), and the maximum of $K_{cat}/K_m$ was found to be at pH 6.5 in MES buffer. The $K_{cat}/K_m$ values at pH 6.5 are comparable in phosphate and MES buffers.

Though many cysteine proteases have maximum activity close to the neutral pH, the acid cysteine proteases have the best activity in the acidic pH range [15] while several other cysteine proteases have activity maxima in the basic pH range (e.g., asclepain cII has pH optima of 9.4–10.2) [16]. Papain is active over a wide range of pHs with maximum

activity often reported in a slightly acidic range. Our data show that PLpro also has a broad pH-activity profile similar to papain with a maximum at pH 6.5. The active site of papain has catalytic cysteine and histidine residues forming a thiolate-imidazolium ion pair. The molecular dynamics simulation of PLpro also shows that the calculated pKa of catalytic residues, C111 and H272 are < 4.5 and > 8.5, respectively [14]. Therefore, the catalytic cysteine and histidine in SARS-CoV-2 PLpro would also exist as an ion-pair over a wide range of pHs and the observed loss of activity below pH 5.5 may not be associated with the protonation states of the catalytic residues, instead some other factors might be responsible.

To further investigate whether the loss in enzymatic activity at acidic pHs is reversible or irreversible, the protein was incubated in 50 mM sodium acetate buffer at pH 4.0, 4.5, and 5.0 for 1 hour. The enzymatic assays were subsequently performed in 50 mM MES, pH 6.5. It was found that incubation at lower pHs completely abolished the catalytic activity, suggesting an irreversible inactivation of the enzyme (Fig. 4a). These observations, together with DSF data suggest that enzyme gets denatured irreversibly below pH 5.5 leading to an observed loss in enzymatic activity. However, similar incubation experiments at basic pHs showed that the enzyme regained catalytic activity when incubated at pHs 8.0 and pH 8.5, suggesting the changes occurring in the enzyme at these pHs are reversible. An irreversible loss of catalytic activity was observed at pH 9.0 and above.

To see the effect of temperature on the enzymatic activity of PLpro, assays were carried out at 25 °C, 30 °C, 37 °C, and 42 °C. It was found that the enzyme has maximum $K_{cat}/K_m$ at 30 °C (Fig. 4b).
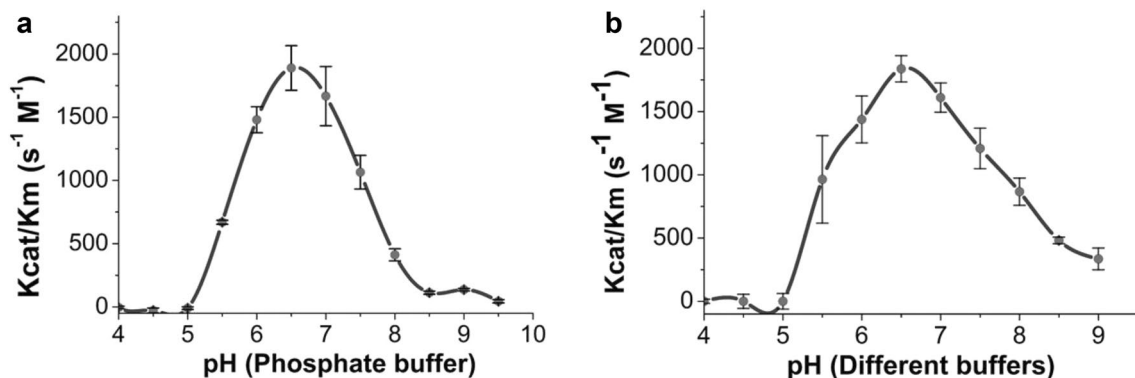


**Fig. 3** Enzyme kinetics at different pHs. **a** Enzymatic efficiencies ($K_{cat}/K_m$) at different pHs of 50 mM phosphate buffer. **b** Enzymatic efficiencies ($K_{cat}/K_m$) at different pHs of 50 mM buffers (Sodium acetate pH 4–5, MES pH 5.5–6.5, HEPES pH 7–7.5, Tris pH 8–9). Experiments were carried out in triplicate at each pH
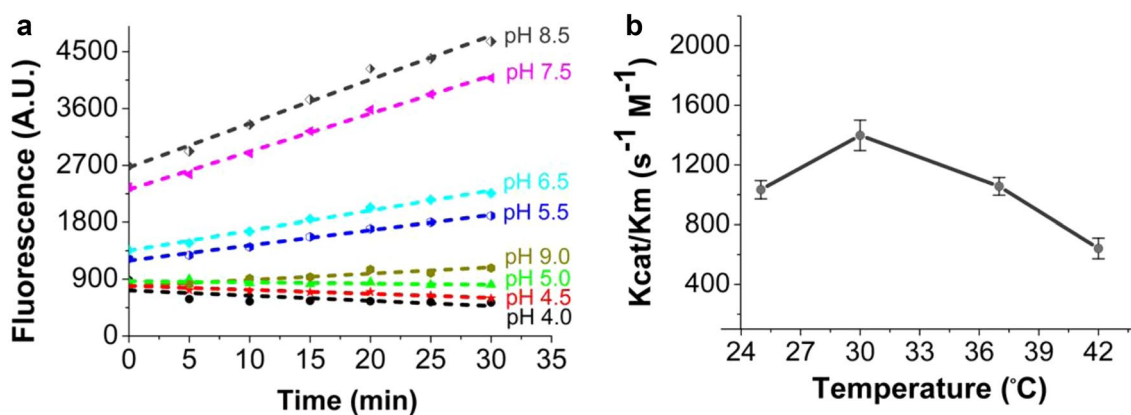
**Fig. 4** **a** Activity regain assay to check reversibility of enzymatic activity at different pHs. The enzyme was incubated in 50 mM buffers of different pHs (Sodium acetate pH 4–5, MES pH 5.5–6.5, HEPES pH 7.5, Tris pH 8.5–9) for 1 h at 4 °C, followed by enzymatic assay in 50 mM MES pH 6.5 at 30 °C. No increase in AMC fluorescence at lower pHs (4–5) and higher pH (9) suggest an irreversible damage to the enzyme. **b** Effect of temperature on enzymatic activity ($K_{cat}/K_m$)



**Fig. 5** Enzyme activity in presence of salt, reducing agent, and additives. $K_{cat}/K_m$ with varying concentration of **a** NaCl (0–500 mM), **b** DTT (0–20 mM), **c** EDTA (0–2 mM), and **d** DMSO (0–10% v/v)
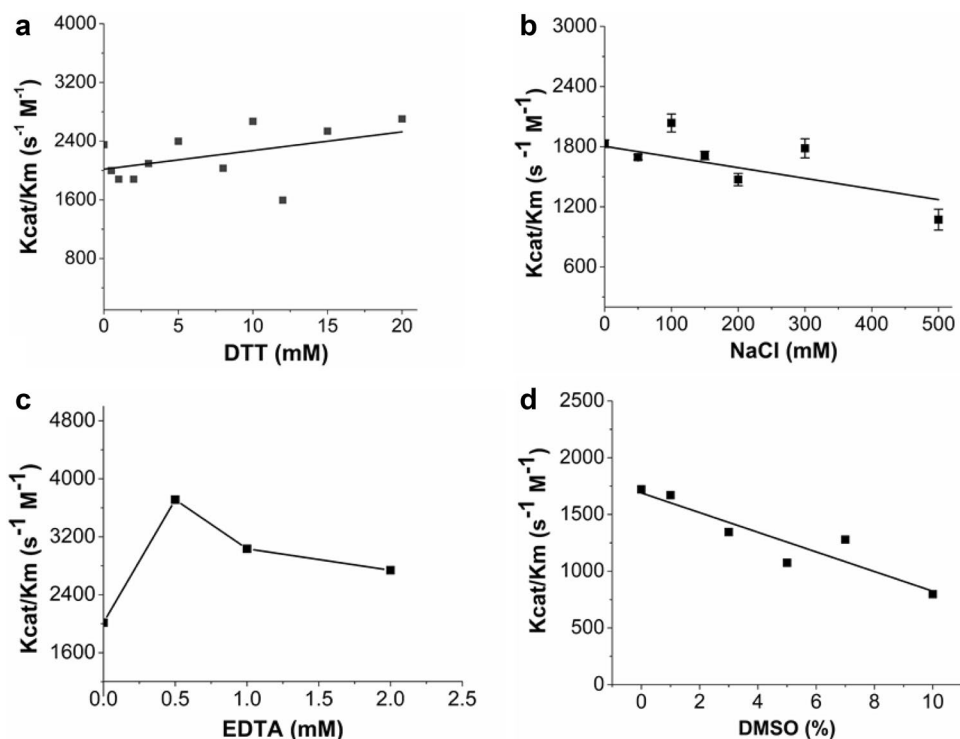
## Effect of DTT and Ionic Strength on Enzymatic Activity

The DLS experiments showed that the reducing agents have a significant effect on the aggregation state of the protein. To explore whether reducing agents have any effect on the enzymatic activity through modification of cysteine residues (including the catalytic cysteine), assays were performed at pH 6.5 using different concentrations of DTT. As seen from Fig. 5a, DTT did not significantly affect the catalytic activity. However, 5 mM DTT in assay buffer has been reported earlier to reduce the non-specific interaction of a ligand with the enzyme during high-throughput inhibitor screening [17]. Therefore, 5 mM DTT in assay buffer should be considered for inhibitor screening. The effect of ionic strength on enzymatic activity was also explored in 50 mM MES buffer pH 6.5 using varying concentrations (0–500 mM) of NaCl. It was found that NaCl also did not have a significant effect on the

enzymatic activity (Fig. 5b). Nonetheless, 100 mM NaCl was found to improve reproducibility of the results.

## Effect of EDTA and DMSO

The enzymatic activity in presence of EDTA and DMSO was measured in 50 mM MES, pH 6.5. EDTA concentrations were varied from 0.5 to 2.0 mM and the best activity was found to be at 0.5 mM EDTA (Fig. 5c). The mechanism by which EDTA enhances enzymatic activity remains elusive. The enzymatic activity was also measured in presence of 1–10% DMSO. Though there was no significant change in the activity up to one percent DMSO, decrease in catalytic activity was observed above one percent DMSO (Fig. 5d).

## Conclusion

To optimize conditions for high-throughput inhibitor screening against SARS-CoV-2 PLpro, the factors affecting stability and activity of the enzyme have been investigated here. The DSF experiments show that at acidic pHs (4.0–5.5), the enzyme partially unfolds giving a high fluorescence signal, whereas near neutral pHs the enzyme was found to be stable. The best stability for long-term storage was seen in a buffer containing 50 mM HEPES pH 7.5, 100 mM NaCl, and 5 mM DTT. The enzymatic activity, however, was found to be the best at pH 6.5. Though the salt and DTT did not significantly affect the enzymatic activity, 100 mM NaCl improved the reproducibility of assay results and 5 mM DTT was considered useful in preventing non-specific binding of a ligand during inhibitor screening. 0.5 mM EDTA was found to increase the enzymatic activity, whereas the activity gradually decreased above 1.0% DMSO. The best condition for the enzymatic assay was found to be at 30 °C in an assay buffer containing 50 mM MES pH 6.5, 100 mM NaCl, 0.5 mM EDTA, 5 mM DTT, 0.1 mg/ml BSA, and less than 1% DMSO.

## Declarations

**Conflict of interest** There are no conflicts to declare.

## References

1. Wang, C., Horby, P. W., Hayden, F. G., & Gao, G. F. (2020). A novel coronavirus outbreak of global health concern. *The Lancet, 395*, 470–473.
2. Hu, B., Guo, H., Zhou, P., & Shi, Z.-L. (2021). Characteristics of SARS-CoV-2 and COVID-19. *Nature Reviews Microbiology, 19*, 141–154.
3. V'kovski, P., Kratzel, A., Steiner, S., Stalder, H., & Thiel, V. (2021). Coronavirus biology and replication: Implications for SARS-CoV-2. *Nature Reviews Microbiology, 19*, 155–170.
4. Gil, C., Ginex, T., Maestro, I., Nozal, V., Barrado-Gil, L., Cuesta-Geijo, M. Á., Urquiza, J., Ramírez, D., Alonso, C., Campillo, N. E., & Martinez, A. (2020). COVID-19: Drug targets and potential treatments. *Journal of Medicinal Chemistry, 63*, 12359–12386.
5. Freitas, B. T., Durie, I. A., Murray, J., Longo, J. E., Miller, H. C., Crich, D., Hogan, R. J., Tripp, R. A., & Pegan, S. D. (2020). Characterization and noncovalent inhibition of the deubiquitinase and deISGylase activity of SARS-CoV-2 papain-like protease. *ACS Infectious Diseases, 6*, 2099–2109.
6. Arya, R., Kumari, S., Pandey, B., Mistry, H., Bihani, S. C., Das, A., Prashar, V., Gupta, G. D., Panicker, L., & Kumar, M. (2021). Structural insights into SARS-CoV-2 proteins. *Journal of Molecular Biology, 433*, 166725.
7. Rut, W., Lv, Z., Zmudzinski, M., Patchett, S., Nayak, D., Snipas, S. J., Oualid, F. E., Huang, T. T., Bekes, M., Drag, M., & Olsen, S. K. (2020). Activity profiling and crystal structures of inhibitor-bound SARS-CoV-2 papain-like protease: A framework for anti–COVID-19 drug design. *Science Advances, 6*, eabd4596.
8. Klemm, T., Ebert, G., Calleja, D. J., Allison, C. C., Richardson, L. W., Bernardini, J. P., Lu, B. G., Kuchel, N. W., Grohmann, C., Shibata, Y., Gan, Z. Y., Cooney, J. P., Doerflinger, M., Au, A. E., Blackmore, T. R., Heden van Noort, G. J., Geurink, P. P., Ovaa, H., Newman, J.,…Komander, D. (2020). Mechanism and inhibition of the papain-like protease, PLpro, of SARS-CoV-2. *The EMBO Journal, 39*, 6275.
9. Shin, D., Mukherjee, R., Grewe, D., Bojkova, D., Baek, K., Bhattacharya, A., Schulz, L., Widera, M., Mehdipour, A. R., Tascher, G., Geurink, P. P., Wilhelm, A., Heden van Noort, G. J., Ovaa, H., Müller, S., Knobeloch, K.-P., Rajalingam, K., Schulman, B. A., Cinatl, J.,…Dikic, I. (2020). Papain-like protease regulates SARS-CoV-2 viral spread and innate immunity. *Nature, 587*, 657–662.
10. Osipiuk, J., Azizi, S.-A., Dvorkin, S., Endres, M., Jedrzejczak, R., Jones, K. A., Kang, S., Kathayat, R. S., Kim, Y., Lisnyak, V. G., Maki, S. L., Nicolaescu, V., Taylor, C. A., Tesar, C., Zhang, Y.-A., Zhou, Z., Randall, G., Michalska, K., Snyder, S. A.,…Joachimiak, A. (2021). Structure of papain-like protease from SARS-CoV-2 and its complexes with non-covalent inhibitors. *Nature Communications, 12*, 743.
11. Gao, X., Qin, B., Chen, P., Zhu, K., Hou, P., Wojdyla, J. A., Wang, M., & Cui, S. (2021). Crystal structure of SARS-CoV-2 papain-like protease. *Acta Pharmaceutica Sinica B, 11*, 237–245.
12. Barretto, N., Jukneliene, D., Ratia, K., Chen, Z., Mesecar, A. D., & Baker, S. C. (2005). The papain-like protease of severe acute respiratory syndrome coronavirus has deubiquitinating activity. *Journal of Virology, 79*, 15189–15198.

13. Ratia, K., Saikatendu, K. S., Santarsiero, B. D., Barretto, N., Baker, S. C., Stevens, R. C., & Mesecar, A. D. (2006). Severe acute respiratory syndrome coronavirus papain-like protease: Structure of a viral deubiquitinating enzyme. *Proceedings of the National academy of Sciences of the United States of America, 103*, 5717–5722.

14. Henderson, J. A., Verma, N., Harris, R. C., Liu, R., & Shen, J. (2020). Assessment of proton-coupled conformational dynamics of SARS and MERS coronavirus papain-like proteases: Implication for designing broad-spectrum antiviral inhibitors. *The Journal of Chemical Physics, 153*, 115101.

15. Yamakami, K., Hamajima, F., Akao, S., & Tadakuma, T. (1995). Purification and characterization of acid cysteine protease from metacercariae of the mammalian trematode parasite *Paragonimus westermani*. *European Journal of Biochemistry, 233*, 490–497.

16. Liggieri, C., Obregón, W., Trejo, S., & Priolo, N. (2009). Biochemical analysis of a papain-like protease isolated from the latex of *Asclepias curassavica* L. *Acta Biochimica et Biophysica Sinica (Shanghai), 41*, 154–162.

17. Ratia, K., Pegan, S., Takayama, J., Sleeman, K., Coughlin, M., Baliji, S., Chaudhuri, R., Fu, W., Prabhakar, B. S., Johnson, M. E., Baker, S. C., Ghosh, A. K., & Mesecar, A. D. (2008). A noncovalent class of papain-like protease/deubiquitinase inhibitors blocks SARS virus replication. *Proceedings of the National academy of Sciences of the United States of America, 105*, 16119–16124.